

Taiyi: A high-performance CKKS accelerator for Practical Fully Homomorphic Encryption

Shengyu Fan^{*†}, Xianglong Deng^{*†}, Zhuoyu Tian^{*†}, Zhicheng Hu[‡],
Liang Chang[‡], Rui Hou^{*†}, Dan Meng^{*†}, Mingzhe Zhang^{*†✉}

^{*}Key Laboratory of Cyberspace Security Defense, Institute of Information Engineering, CAS, Beijing, China.

[†]School of Cyber Security, University of Chinese Academy of Sciences, Beijing, China.

[‡]University of Electronic Science and Technology of China.

Abstract—Fully Homomorphic Encryption (FHE), a novel cryptographic theory enabling computation directly on ciphertext data, offers significant security benefits but is hampered by substantial performance overhead. In recent years, a series of accelerator designs have significantly enhanced the performance of FHE applications, bringing them closer to real-world applicability. However, these accelerators face challenges related to large on-chip memory and area. Additionally, FHE algorithms undergo rapid development, rendering the previous accelerator designs less perfectly adapted to the evolving landscape of optimized FHE applications.

In this paper, we conducted a detailed analysis of existing applications with the new FHE method, making two key observations: 1) the bottleneck of FHE applications shifts from NTT to the inner-product operation, and 2) the optimal α of KeySwitch changes with the decrease in multiplicative level. Based on these observations, we designed an accelerator named *Taiyi*, which includes specific hardware for the inner-product operation and optimizes the NTT and BConv operations through algorithmic derivation. A comparative evaluation of *Taiyi* against previous state-of-the-art designs reveals an average performance improvement of 1.5 \times and reduces the area overhead by 15.7%.

I. INTRODUCTION

Fully Homomorphic Encryption (FHE) enables direct computation on encrypted data, offering a powerful means to safeguard private information. Various FHE schemes have been proposed to cater to different application scenarios, including BGV [6], BFV [4], [7], [13], CKKS [10], and TFHE [11], [29]. Among these, CKKS allows for computations on complex numbers in real-world applications and supports parallel processing of many slots [5], [9], [30]. Consequently, CKKS holds significant promise for the practical application of FHE in real-world scenarios. For the CKKS scheme, the initial step involves encoding a vector containing multiple complex values into plaintext using the FHE compiler, and then the plaintext undergoes encryption. Once encrypted, CKKS allows for direct multiplication and other linear arithmetic operations on the ciphertexts. The decryption and decoding phase is where the ciphertext is ultimately decrypted, and the outputs of this phase are the ultimately computed results.

The CKKS strategy, while powerful, faces significant computational overhead, posing challenges to the speed of applica-

tion execution and hindering the practical deployment of FHE applications. Various methods have been proposed to address this issue and enhance FHE application performance across different platforms. On GPU platforms, strategies include algorithm optimization, bandwidth optimization, and the use of Tensor Cores to reduce the execution time of FHE applications [14], [21]. Similarly, on FPGA platforms, methods involve optimizing dataflow and implementing modular fusion techniques to enhance the efficiency of FHE operations [34], [40]. Despite these advancements, a substantial performance gap still exists, impeding the realization of FHE applications. Consequently, domain-specific accelerators have been introduced to narrow this performance gap in real-world applications. These accelerators deploy specialized components for FHE arithmetic kernels, achieving high throughput and overall performance improvements for FHE applications [22], [23], [25], [35], [36]. Therefore, domain-specific accelerators contribute significantly to achieving optimal performance for FHE applications, a crucial step towards making FHE a practical reality in our lives in the future.

While existing FHE accelerators have showcased remarkable performance in executing FHE applications, the state-of-the-art implementation of *SHARP* is particularly noteworthy. It has demonstrated significant performance improvements compared to CPU implementations and notable reductions in both area and on-chip storage when contrasted with previous accelerator solutions [22]. However, the FHE algorithms undergo rapid development, which presents new challenges for existing accelerators during execution.

The recent algorithm-level optimizations for the CKKS scheme significantly enhance application performance by reducing the execution times of specific arithmetic kernels. Thus, the KLSS method decreases the execution times of the NTT, causing a significant change in the bottleneck [19], [24]. Consequently, it needs to re-analyze both FHE applications and the parameter selection of the CKKS scheme, prompting a re-design of the FHE accelerator to align with the evolving landscape of FHE algorithm-level optimization.

This work focuses on optimizing performance for the KLSS-based method on the accelerator. We comprehensively analyze the KLSS method's characteristics, performing a runtime state analysis on the *SHARP* accelerator. Key observations

Corresponding Author: Mingzhe Zhang (zhangmingzhe@iie.ac.cn).

include a shift in crucial operations, with *Inner Product* (IP) operations gaining prominence over the previously dominant Number Theoretic Transform (NTT). Despite the performance of NTT’s continued importance, efficient execution hinges on addressing the challenges posed by IP operations, where a substantial accumulation of instructions in existing accelerators impedes performance. Furthermore, our exploration underscores the suboptimal nature of conventional parameter selection with a fixed α to the optimal α dynamically changes with multiplication depth consumption.

To address the challenges inherent in KLSS-based methods, we present several optimizations to enhance the performance of FHE applications. Our contributions are as follows:

- **We bridge computer architecture design and timely cryptography** research. Prior FHE accelerator research focused on improving classical FHE scheme performance, assuming FHE algorithm changes are transparent to hardware. This paper demonstrates that specific FHE algorithm development poses challenges to existing accelerator architecture but also offers new optimization opportunities. Considering cryptography’s timely progress, accelerator architecture optimization can significantly improve performance without increasing hardware overhead. This work highlights the importance of tracking cryptography’s latest progress and may inspire new ideas for future FHE accelerators.
- **We design dedicated hardware structures and acceleration schemes to address the new performance bottlenecks (IP and BConv) identified in the experimental analysis.** For IPs, we propose a hierarchical MAC structure (HPIP) and enhance data reuse through dataflow optimization. For BConvs, we propose the fusion method to reduce BConv in Recover-limbs stages and the ModDown.
- **We prove that the proper parameter selection significantly affects the CKKS performance and provides a new direction for the optimization of the FHE compiler.** We propose a dynamic parameter selection scheme and then experimentally analyze the impact of various parameter values. This will probably inspire more work on the optimization of compiler and accelerator for FHE workloads.
- **Comprehensive Evaluation of Taiyi:** We offer a comprehensive evaluation of *Taiyi* from diverse perspectives. The assessment results underscore the efficacy of our accelerator design for KLSS-based FHE applications, showcasing the $1.5\times$ performance improvement across various application scenarios on average.

These contributions collectively address critical aspects of KLSS-based FHE methods, spanning both hardware and algorithmic domains, focusing on achieving superior performance for the FHE applications.

II. BACKGROUND

In this section, we introduce the background related to this paper. Moreover, the symbols related to this paper are

TABLE I
THE MAXIMUM $\log PQ$ AND CORRESPONDING TARGET LEVELS TO ACHIEVE 128-BIT SECURITY FOR DIFFERENT DEGREES.

N	h	$\log PQ$	λ	L_{target}
2^{15}	512	782	134.4	22
2^{16}	512	1656	133.0	45
2^{17}	512	3276	134.5	91
2^{18}	512	6804	128.3	189

indicated in Table II.

A. CKKS: A Practical and Promising FHE Scheme

Cryptographic schemes play a crucial role in safeguarding real-world data within the privacy and information protection domain. However, the complex operations involved in CKKS pose a significant challenge, making integrating this scheme with practical applications difficult. This section provides a brief overview of the CKKS scheme hierarchy to help readers understand the different layers and their relationships.

The hierarchy of the CKKS is as follows.

- **BOOT** layer. It facilitates the recovery of the multiplicative level of ciphertexts through the *Bootstrapping* operation, directly interfacing with the *HEOp* layer. The *Bootstrapping* operation involves multiple *HMULT* and *HROTATE* operations in the *HEOp* layer to achieve homomorphic decoding and encoding.
- **HEOp** layer. It encompasses fundamental operations used in CKKS, including *HMULT*, *HROTATE*, *HADD*, *PMULT*, and *PADD*. It serves as a pivotal component of the CKKS scheme, accessing the *Arithmetic* layer for all operations and requiring access to the *KSW* layer for *HMULT* and *HROTATE* operations.
- **KSW** layer. It is dedicated to serving the layers above it and incurs significant computational cost due to executing NTT, BCONV, and IP operations.
- **Arithmetic** layer. It houses all arithmetic kernels, with each kernel serving the *KeySwitch* operation and supporting basic arithmetic operations (*ADD* and *MUL*) for operations in the *HEOp* layer.

Applications secured with CKKS interact directly with the *BOOT* and *HEOp* layers, where original application operations transform into linear operations in FHE, including *HMULT* and *CMULT*. It also incorporates the *Bootstrapping* operation to refresh the multiplicative level.

Based on the above description, the *KSW* layer plays a pivotal role in the CKKS hierarchy, acting as the bridge between FHE operations and arithmetic kernels. This layer significantly impacts the overall performance of FHE applications. The prominent performance bottleneck in CKKS arises from its considerable computational overhead. To address this challenge, we introduce a specialized accelerator designed to optimize performance, emphasizing enhancing the efficiency of the *KeySwitch* operation and, consequently, improving overall application efficiency.

B. CKKS parameters

CKKS is a homomorphic encryption scheme that relies on lattice cryptography. Hence it is influenced by parameters such

Algorithm 1: Hybrid KeySwitch method

Require: $\mathbf{c} = \{\hat{\mathbf{c}}_0, \dots, \hat{\mathbf{c}}_\beta\}$, $M=N\log N$, $L=\alpha\beta$

- 1: **for** i in 0 to β **do**
- 2: $\hat{\mathbf{c}}_i = \{\hat{c}_i^0, \dots, \hat{c}_i^L\} \leftarrow \text{NTT}(\text{BConv}(c_i^0, \dots, c_i^\alpha))$
- 3: **end for**
- 4: \triangleright *Decomposition* ($O((M + \alpha)L\beta)$)
- 5: **for** j in 0 to 2 **do**
- 6: **for** n in 0 to β **do**
- 7: $\tilde{\mathbf{c}}_m^j += \hat{c}_n * \text{evk}_{mn}^j$
- 8: **end for**
- 9: \triangleright (*IP* $O(\beta LN)$)
- 10: $\tilde{\mathbf{c}}^j = \{\tilde{c}_i^0, \dots, \tilde{c}_i^L\} \leftarrow \text{INTT}(\tilde{\mathbf{c}}_m^j)$
- 11: \triangleright *Recover-form* ($O(ML)$)
- 12: **end for**
- 13: **return** $\text{ModDown}(\hat{\mathbf{c}}^0, \hat{\mathbf{c}}^1)$

as the lattice dimension N and modulus PQ . The increment of N enhances the security level λ , while the increment in PQ results in a reduction of λ . In the CKKS scheme, P represents the special moduli product, and Q stands for the ciphertext moduli product, both of which are correlated with L and K , ($L + K = \frac{\log(PQ)}{\text{word length}}$). As shown in Table I, to achieve 128-bit security for FHE, we employ an estimation tool [16] to calculate the maximum allowable value of PQ for the most commonly used values of N . Additionally, PQ is influenced by parameters such as L and K , with K is determined by $\lceil \frac{L+1}{d_{\text{num}}} \rceil$. Consequently, we adopt a word length of 36 bits¹, as recommended in [22]. This choice allows us to derive the target level L_{target} from PQ , which is also equivalent to $L + K$. We establish a relationship between d_{num} and maximum level,

$$L = \lfloor \frac{d_{\text{num}} * L_{\text{target}} - 1}{d_{\text{num}} + 1} \rfloor \quad (1)$$

It enables us to identify the optimal value of d_{num} for various degrees of N while ensuring a security level of $\lambda > 128$.

C. KLSS: A Breakthrough KeySwitch Method

KeySwitch operation significantly impacts the runtime of FHE applications, constituting the majority of the overall execution time [18], [23], [24], [35]. Ref. [18] introduced a hybrid KeySwitch method to balance P and Q for minimal execution times in arithmetic kernels, as shown in Alg. 1. However, this method remains time-consuming, particularly during NTT operations, leading to significant delays in overall FHE application execution. To enhance the KeySwitch operation's performance further, a new method named KLSS, illustrated in Alg. 2, focuses on reducing NTT execution times through RNS-based gadget decomposition [24]. This approach computes the same formula differently from the previous

¹According to Ref. [22], a 36-bit word length is considered the minimum requirement to meet the precision needs of FHE applications. Nevertheless, increasing word length becomes necessary in scenarios where precision requirements are heightened. However, the maximum level analysis method proposed in this paper remains applicable in such cases.

Algorithm 2: KLSS KeySwitch method

Require: $\mathbf{c} = \{\hat{\mathbf{c}}_0, \dots, \hat{\mathbf{c}}_\beta\}$, $M=N\log N$

- 1: **for** i in 0 to β **do**
- 2: $\hat{\mathbf{c}}_i = \{\hat{c}_i^0, \dots, \hat{c}_i^{\alpha'}\} \leftarrow \text{NTT}(\text{BConv}(c_i^0, \dots, c_i^\alpha))$
- 3: **end for**
- 4: \triangleright *Gadget-decomp* ($O((M + \alpha)\alpha'\beta)$)
- 5: **for** j in 0 to 2 **do**
- 6: **for** m in 0 to $\tilde{\beta}$ **do**
- 7: **for** n in 0 to β **do**
- 8: $\tilde{\mathbf{c}}_m^j += \hat{c}_n * \text{evk}_{mn}^j$
- 9: **end for**
- 10: \triangleright (*IP* $O(\beta\tilde{\beta}\alpha'N)$)
- 11: $\tilde{\mathbf{c}}_i^j = \{\tilde{c}_i^0, \dots, \tilde{c}_i^\alpha\} \leftarrow \text{BConv}(\text{INTT}(\tilde{\mathbf{c}}_m^j))$
- 12: \triangleright *Recover-Limbs* ($O((M + \alpha)\alpha'\tilde{\beta})$)
- 13: **end for**
- 14: **end for**
- 15: **return** $\text{ModDown}(\hat{\mathbf{c}}^0, \hat{\mathbf{c}}^1)$

KeySwitch method, avoiding additional noise growth during computation. Consequently, KLSS can be directly applied to various FHE applications, achieving further performance improvement without introducing additional noise impact. As shown in Alg. 2, KLSS consists of four main steps: *Gadget-decomp*, *Inner-Product (IP)*, *Recover-Limbs*, and *ModDown*.

As shown in Alg. 2, the first step (*Gadget-decomp*) is performed using the BConv and NTT operations. All limbs are grouped into β groups, each containing α limbs. Compared to the previous KeySwitch method shown in Alg. 1, this step significantly reduces the number of NTT-related operations from $\alpha\beta^2$ to $\beta\alpha'$ times by grouping ciphertext into small groups. Additionally, it alters the scale for each BConv operation from $\alpha\beta$ to α' . As a result, this step substantially reduces the computational overhead, leading to improved performance.

The second step involves IP operations, which multiplies a vector of polynomial groups by a matrix of polynomial groups. Compared to the hybrid KeySwitch method, this step significantly increases computational complexity from $\alpha\beta^2$ to $\beta\tilde{\beta}(\alpha')^2$, becoming the primary bottleneck of the entire KeySwitch operation. Efficiently executing the IP operation is crucial for improving KeySwitch performance.

The *Recover-Limbs* stage is responsible for restoring the number of limbs for the ciphertext. Each group executes a BConv operation to convert the limbs back into the corresponding levels of the original limbs. This step closely resembles the hybrid KeySwitch operation and also involves NTT and BConv operations. However, in comparison to the previous method, the *Recover-Limbs* stage is an additional step, which increases the number of BConv operations by $\tilde{\beta}$ times, each converting from α' limbs to α limbs.

In summary, the KLSS method significantly improves the performance of KeySwitch by reducing the number of NTT operations. However, it also increases the computational

complexity of the BConv and IP operations. In this paper, we conducted a detailed runtime analysis on the new algorithm and designed specific hardware and algorithm optimizations. These optimizations led to a reduction in the overhead of BConv and IP.

D. Four-Step NTT algorithm

Previous designs prioritized NTT operation for overall FHE application execution [22], [23], [25], [35], [40]. The 4-step NTT method meets vector requirements and enhances batch processing. While enhancing NTTU, these methods added complexities, demanding a comprehensive understanding of the algorithmic process and specific *twiddle-factor* requirements. This section offers an overview of 4-step NTT methods, focusing on algorithmic aspects.

$$X_k = \sum_{n=0}^{N-1} x_n W_{2N}^{2nk+n} \quad (2)$$

Based on the standard NTT formula given in Eq. 2, we can infer the formula for the four-step NTT. Thus, the formula is as follows:

$$X_{k_1+N_1k_2} = \sum_{n_2=0}^{N_2-1} \sum_{n_1=0}^{N_1-1} x_{n_1N_2+n_2} W_{2N}^{(n_1N_2+n_2)(2(k_1+N_1k_2)+1)} \quad (3)$$

where,

$$\begin{aligned} n &= n_1N_2 + n_2 \\ k &= k_1 + k_2N_2 \end{aligned} \quad (4)$$

Now, if we simplify the exponential, and we can get:

$$\begin{aligned} &W_{2N}^{(n_1N_2+n_2)(2(k_1+N_1k_2)+1)} \\ &= W_{2N}^{2k_1n_2+n_2+(2k_1+1)n_1N_2+2k_2n_1N+2N_1k_2n_2} \\ &= W_{2N_1}^{2k_1n_1+n_1} W_{2N_2}^{k_2n_2} \cdot 1 \cdot W_{2N}^{2k_1n_2+n_2} \end{aligned} \quad (5)$$

Therefore, the four-step formula is summarized as follows.

$$\begin{aligned} &X_{k_1+N_1k_2} \\ &= \sum_{n_2=0}^{N_2-1} \sum_{n_1=0}^{N_1-1} x_{n_1N_2+n_2} W_{2N_1}^{2k_1n_1+n_1} W_{2N_2}^{k_2n_2} W_{2N}^{2k_1n_2+n_2} \end{aligned} \quad (6)$$

Eq. 6 outlines the NTT operation's four steps: N_1 -NTT, Transpose, Hadamard Product, and N_2 -NTT. In the N_1 -NTT operation, the twiddle-factor for the i -th Butterfly Unit in each stage (s) is $W_{2N_1}^{2^s+i}$. For the N_2 -NTT operation, the twiddle-factor for the i -th Butterfly Unit is $W_{2N_2}^i$, and consistent across all NTT stages.

Moreover, the previous accelerator optimized the 4-step NTT method into a 10-step process to reduce global communication during execution [22]. However, this introduces additional overhead due to changing requirements for the twiddle factor, leading to increased pipeline stalls. In this paper, we introduce a new NTT method based on the 4-step NTT through algorithmic inference, significantly mitigating the additional overhead of the 10-step NTT.

TABLE II
SYMBOLS AND NOTIONS USED IN THIS PAPER.

Symbol	Definition
λ	Security parameters for the FHE.
Q	The product of all prime modulus values, denoted by $\prod_{i=0}^L q_i$.
P	The product of special (prime) moduli, denoted by $\prod_{k=0}^K p_k$.
T	The product of prime moduli, mutually exclusive with P.
PQ	The maximum moduli of the lattice.
L	The maximum multiplicative level, which is related to Q.
N	Degree of a polynomial and the lattice dimension.
l	Current multiplicative level
d_{num}	The number of digits in the switching key. [18]
α	$\alpha = \lceil \frac{l+1}{d_{\text{num}}} \rceil$, Number of limbs that comprise a single digit in the KeySwitch decomposition ($K=\alpha$).
β	$\beta = \lceil \frac{l+1}{\alpha} \rceil$. l limbs polynomials are split into β groups. this number of digits during base decomposition.
α'	The number of limbs in R^T , which used in KLSS-method.
$\tilde{\beta}$	The groups of limbs used in IP, which is $\lceil \frac{l+\alpha+1}{\alpha} \rceil$.
fftIter	Multiplicative depth of a linear transform in bootstrapping.

E. Overview of Previous FHE Accelerators

To enhance the performance of CKKS, previous efforts involved designing domain-specific accelerators with customized functional units optimized for specific arithmetic kernels [22], [23], [25], [35], [36]. We briefly introduce the functional previous design for the main component as follows:

- **NTT**: NTT component executes *NTT*-related kernels, including *Butterfly* and *transpose* units. The *ten-step* method, considered state-of-the-art, reduces communication within the NTT component by optimizing the algorithm [22]. However, pipeline stalls still occurred due to necessary twiddle-factor modifications during execution. Our algorithm optimization aims to eliminate these stalls to further improve performance.
- **BConv**: The *Basis Conversion* operation can be divided into two steps: the first step involves element-wise multiplication, while the second step consists of a matrix-vector multiplication operation. For the second step, the BConv component is designed to facilitate parallel computing with multiple MAC units. Consequently, this stage can be rapidly executed in parallel by leveraging a large number of MAC computing units [22], [23].
- **AUTOU**: The *Automorphism* operation involves moving data based on the mapping index, which can be an irregular permutation among all N coefficients. This operation is particularly useful for encoded ciphertexts, as it allows for coefficient rotation without decryption. The rotation is performed by the AUTOU unit, which consists of several MUX units arranged in eight stages. This component includes internal permutation logic to ensure high performance during related operations [23].
- **EWE**: Element-Wise Engine (EWE) component processes various element-wise operations, including the Hadamard Product used by Basis Conversion, ADD, or MUL operations. It also serves the IP operation in the previous accelerator, as the execution time of the IP operation is relatively low in the traditional KeySwitch method.

While previous efforts have notably improved CKKS ap-

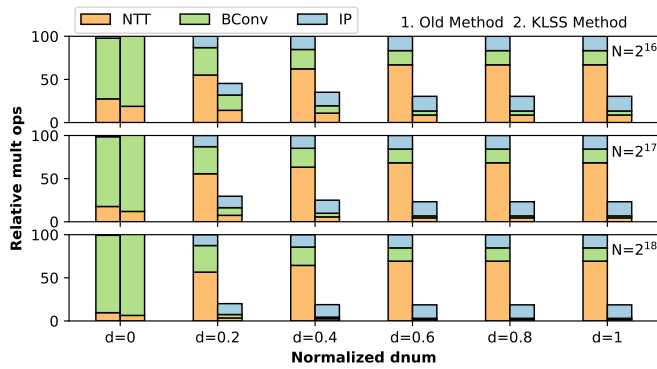


Fig. 1. Computational arithmetic multiplication number breakdown. Results are measured for all possible values of d_{num} and N .

TABLE III

FOR THE SMALL d_{NUM} PARAMETER, THE KLSS METHOD REDUCES THE TOTAL NUMBER OF MULTIPLICATION OPERATIONS COMPARED TO THE PREVIOUS `KeySwitch` METHOD.

	$N=16$	$N=17$	$N=18$
$d_{\text{num}}=2$	1.06	1.12	1.17
$d_{\text{num}}=3$	9.9%	5.7%	6.4%
$d_{\text{num}}=4$	23.8%	20.6%	17.3%
$d_{\text{num}}=5$	34.1	32.3%	29.9%

plication performance, the optimization of the KLSS method has brought significant changes to FHE application execution. While previous accelerators performed well, they faced challenges when executing the KLSS-based `KeySwitch`. In this paper, we conduct a detailed analysis of KLSS-based CKKS applications and optimize the components accordingly to align with the rapid development of the CKKS algorithm.

III. MOTIVATION

In this section, we conduct an in-depth analysis of its computational distinctions compared to the previous method [18], we achieve some observations and opportunities for designing an accelerator with the KLSS-based method.

A. Contrasting Computation Workload and Memory Requirements

The KLSS method is a novel `KeySwitch` method, significantly improving the FHE application performance by reducing the execution times of NTT [24]. To discern the difference between KLSS and the previous methods from a hardware perspective, we comprehensively analyze computational complexity breakdowns and memory requirements for both `KeySwitch` methods.

As shown in Figure 1 and Tabel III², a stark contrast emerges between the KLSS method and its predecessor in the proportional relationships of NTT, BConv, and IP operations. KLSS achieves a remarkable reduction in the number of multiplication times for NTT by 59.6%, leading to a 3.6 \times performance enhancement. However, IP and BConv operations within KLSS show are also increased, where IP surging by 44.3% and BConv experiencing a noteworthy average proportion increase. The number of multiplication operations in IP

²Normalized $d = 0$ means $d_{\text{num}} = 1$, and normalized $d = 1$ means $d_{\text{num}} = \text{maximum}$ for each N . Figure 2 and Table IV also use this description.

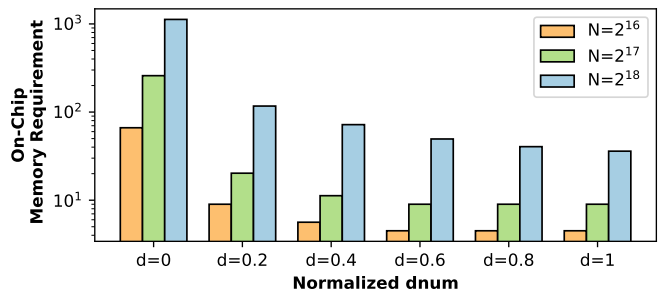


Fig. 2. The On-Chip Memory Requirement for the KLSS-based `KeySwitch` method for IP operation.

TABLE IV

$T_{\text{MULT,A/SLOT}}$ ARE MEASURED FOR ALL POSSIBLE INTEGER d_{NUM} VALUES FOR EACH N AND SATISFY THE SECURITY REQUIREMENT OF $\lambda > 128$.

	$N=2^{16}$	$N=2^{17}$	$N=2^{18}$
$d=0$	28.97	190.22	1665.57
$d=0.2$	18.76	97.35	639.20
$d=0.4$	20.82	119.80	897.82
$d=0.6$	25.43	157.40	1246.74
$d=0.8$	25.43	157.40	1246.74
$d=1$	25.43	157.40	1246.74

increases on average by 3.2%, and BConv experiences a rise of 19.3% in some cases. Compared to the previous method, KLSS presents a notably distinct distribution of computational complexity. Traditionally, emphasizing the optimization of NTT performance in prior hardware accelerators([22], [23], [25], [35], [36]) may not yield substantial benefits in FHE acceleration when employing the KLSS method.

As shown in Figure 2, we note the difference in memory requirements for the IP operation in KLSS compared to the previous method. Each group needs to concurrently compute $\beta \times \alpha'$ ciphertexts in the KLSS-based method, which requires an average of 102.9 MB of memory. In contrast, the previous accelerator processes only α ciphertexts per group. This results in potential challenges related to re-fetching the same ciphertext during the IP operation, leading to additional computational and memory overhead.

The observations indicate a significant challenge for the previous accelerator when executing FHE applications optimized with the KLSS method. Initially designed with a focus on powerful NTT units, the prior accelerator faces a mismatch in computational complexity, since IP becomes the most complex operation. The IP operation incurs additional computational and memory overhead on the previous accelerator due to its sequential computation at the ciphertext group level, lacking parallel processing capabilities. Consequently, there is a need to reconsider FHE accelerator design, particularly in light of the emerging `KeySwitch` method, to achieve further performance enhancements for FHE applications.

B. Performance Analysis and Optimal CKKS Parameter Selection

The FHE application's performance is intricately related to its parameters. Previous research introduced the *amortized multiplication time per slot* ($T_{\text{mult,a/slot}}$) as a metric to identify

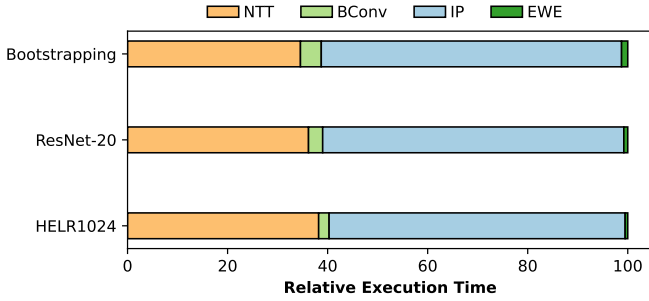


Fig. 3. KeySwitch Execution Time Breakdown in FHE Application Using the KLSS-based method. The KeySwitch execution time constitutes 73.7%, 85.5%, and 84.9% of the total execution time for the respective cases.

optimal parameters [21], which is defined as:

$$T_{\text{mult},a/\text{slot}} = \frac{T_{\text{boot}} + \sum_{l=1}^{L-L_{\text{boot}}} T_{\text{mult}}^{(l)}}{L - L_{\text{boot}}} \cdot \frac{2}{N}$$

where T_{boot} is bootstrapping time and $T_{\text{mult},a/\text{slot}}$ represents the time for HMult at level l . Both T_{boot} and T_{mult} impact the KeySwitch operation. The unique computational behavior of the KLSS method necessitates a re-evaluation of CKKS parameters for optimal performance.

For Bootstrapping, our focus is on determining the fftIter parameter, representing the iterations for homomorphic DFT [8]. To ensure optimal performance, we set fftIter to 6, aligning with recommendations from advanced research [2], [12]. we calculate L_{boot} as $2 \times \text{fftIter} + 9 = 21$, signifying that the maximum level must exceed 21 to meet security and multiplicative depth requirements.

As discussed in the section II-B, the security of FHE is intricately related to the parameters N and PQ . As N increases, the security level λ is enhanced, whereas an increase in PQ leads to a reduction in λ . A larger value of PQ facilitates more multiplicative operations, thereby reducing the necessity for executing the Bootstrapping operation in FHE applications. These observations underscore the crucial role that parameter selection plays in achieving the desired security and performance characteristics.

As shown in Eq. 1, considering the relationship between L and d_{num} , we evaluate the performance of $T_{\text{mult},a/\text{slot}}$ for different degrees³. Table IV presents $T_{\text{mult},a/\text{slot}}$ values for the FHE accelerator with the KLSS method. Thus, we can get the best performance for each N , which achieves 18.76ns, 97.35ns, and 639.2ns for $(2^{16}, 38, 6)$, $(2^{17}, 86, 18)$ and $(2^{18}, 194, 39)$, respectively. Notably, N at 2^{15} yields only one multiplicative level apart from L_{boot} , potentially unsuitable for FHE with Bootstrapping. Besides, settings with $N > 2^{16}$ demand excessive computational resources. Thus, our parameter used in this work is $N = 2^{16}$.

In this paper, to design a more suitable FHE accelerator for the KLSS method, we illustrate our method using the CKKS instance with $N = 2^{16}$, $L = 38$, and $d_{\text{num}} = 6$.

³To address pipeline overlap and component parallelization influences, we sequentially measure execution time for each compartment. These effects are contingent on computational component design, introducing a potential disparity between execution time and computational complexity, thus influencing parameter selection [18], [25].

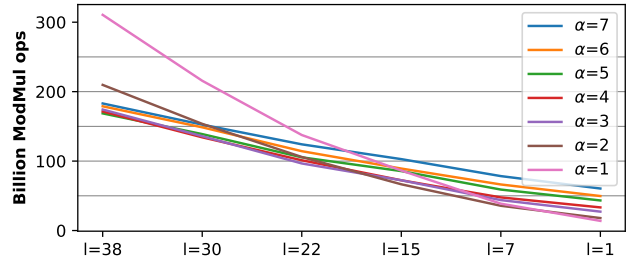


Fig. 4. The relationship between the number of ModMul operations and the decrease of multiplicative level (l). α is the number of single digits.

C. Real-world application breakdown analysis

To gain a more detailed understanding of the bottlenecks associated with the KLSS method in previous accelerators, we develop a simulator based on the SimFHE [2], and modeling the **SHARP** architecture for executing optimized FHE applications with the KLSS method. As illustrated in Figure 3, we observe that the IP operation constitutes the majority of the processing time in the overall application. The heightened computational workload of the IP operation can account for most of the execution time of the EWE component. Consequently, we can infer that the bottleneck of the FHE application has shifted from the NTT operation to the IP operation. The proportion of NTT operation only achieves 36.3% on average, while the proportion of IP operation achieves 59.8% on average and reaches 60.2% for the ResNet-20 application. Our analysis suggests that the majority of IP instructions are constrained by the limited computation component of the **SHARP** accelerator. This limitation significantly impacts the execution efficiency, particularly as IP operations become a predominant factor in the overall workload.

In summary, the previous FHE accelerator is not well-suited to the new changes in the FHE algorithm. Therefore, it is necessary to meet the high computational requirement of IP by re-designing the FHE accelerator.

D. Diverging the best α for different multiplicative level

As detailed in Section III-B, the parameter d_{num} is fixed before FHE operations, determining the corresponding α for the KeySwitch operation. Our analysis establishes the optimal d_{num} for security and maximal multiplicative level L . However, HMULT and CMULT reduce the multiplicative level budget, affecting NTT and Hadamard Product execution times. Figure 4 illustrates that, for KLSS, the optimal α changes as l decreases. In real-world FHE workloads, where l decreases, a fixed α may not yield optimal performance. To enhance performance for dynamic multiplicative levels, we propose dynamic α adjustment. Prior studies [19] also affirm that dynamic α selection optimizes KeySwitch performance. Thus, in this paper, we propose a static compiler to dynamic select α for further improving the performance of KLSS-based FHE applications.

E. Opportunities

Based on the above observations, we conclude our opportunities to design the new FHE accelerator as follows:

- The KLSS-optimized FHE operation, as discussed in Sections III-A and III-C, significantly reduces the computational workload while increasing demands on the IP operation. This underscores the imperative need for dedicated hardware to support IP, along with the development of an optimized data flow to reduce memory requirements. Additionally, there is a necessity for further optimizing the NTT component due to its high overhead.
- The BConv operation, as outlined in Sections III-C and III-A, experiences increased execution time with KLSS-based KeySwitch. Algorithmic optimizations are essential to alleviate redundant BConv operations.
- Sections III-B and III-D highlight the ability to select optimal values for L and d_{num} to meet security requirements. Developing a static compiler to further optimize FHE application performance is crucial to determining the ideal α for each multiplicative level. This compiler should analyze consumption at the FHE application level and set the optimal α .

Based on the above opportunities, we propose a specific accelerator, named *Taiyi*, which improves the performance of KLSS-based FHE applications by algorithm optimization and hardware design. The following section briefly introduces our domain-specific architectures and algorithm optimizations.

IV. DESIGN

To improve the performance of KLSS-based FHE applications, we analyze hardware behavior and develop *Taiyi*, an optimized accelerator. Focusing on critical aspects of the KLSS-based method, we design specific components, refine data flow, and introduce a compiler for customized instruction generation at various levels of multiplication. By implementing this comprehensive approach, the efficiency and overall performance of KLSS-based FHE applications are improved.

A. Multi-step (1)NTT Architecture

While the prominence of NTT has diminished in KLSS-based FHE applications, it remains crucial, serving as a bridge between BCONV and IP operations. In this section, we introduce optimizations for the NTT operation through algorithm derivation.

In this section, we propose the Multi-step method to perform NTT operation, which is an extension of the four-step NTT method. Based on Eq. 6, the multi-step NTT comprises N_1 -NTT and N_2 -NTT, each with four steps, minimizing on-chip communication during computation. Additionally, the new twiddle factor generation scheme eliminates the pipeline stall caused by updating the second-stage twiddle factor in Sharp [22]. In N_1 -NTT, the exponent of the *Twiddle-factor* ($W_{2N_1}^{2k_1 n_1 + n_1}$) mirrors that of the standard NTT (W_{2N}^{2nk+n}), with the base changing from N to N_1 . However, the *Twiddle-factor* for N_2 -NTT differs from the previous operation. Subsequently, adhering to the basic formula, we will restate the formulation for the N_2 -NTT operation.

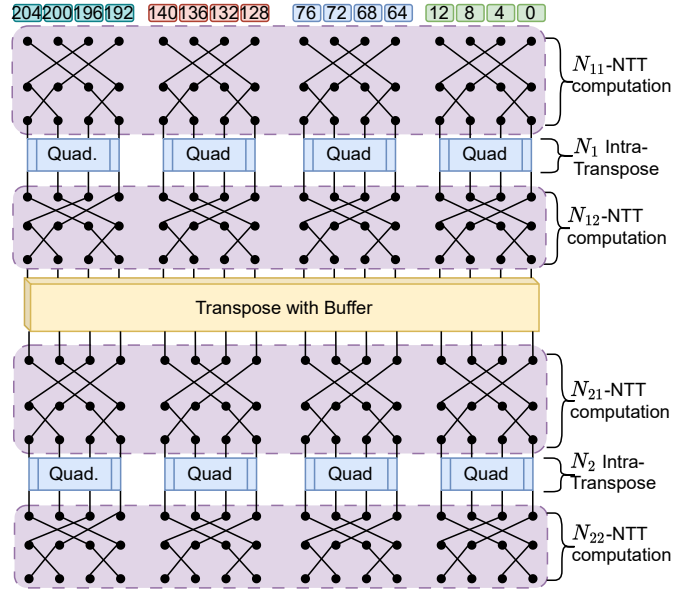


Fig. 5. Organization of the NTTU and the data-map for input polynomial. Each NTTU serves 256 elements in one cycle, and *Taiyi* contains 16 lanes and each lane processes 16 elements on one cluster. For simplicity, here we take $M=4$ for each NTTU group as an example.

$$X_{k_2} = \sum_{n_2=0}^{N_2-1} x_{n_2} W_{2N_2}^{2n_2 k_2} \quad (7)$$

Therefore, the four-step NTT formula for N_2 is as follows:

$$\begin{aligned} & X_{k_{21} + N_{21} k_{22}} \\ &= \sum_{n_{22}=0}^{N_{22}-1} \sum_{n_{21}=0}^{N_{21}-1} x_{n_{21} N_{22} + n_{22}} W_{2N_2}^{2(n_{21} N_{22} + n_{22})(k_{21} + N_{21} k_{22})} \\ &= \sum_{n_{22}=0}^{N_{22}-1} \sum_{n_{21}=0}^{N_{21}-1} x_{n_{21} N_{22} + n_{22}} W_{2N_{21}}^{2n_{21} k_{21}} W_{2N_{22}}^{2n_{22} k_{22}} W_{2N_2}^{n_{22} k_{22}} \end{aligned} \quad (8)$$

In both the N_{21} -NTT and N_{22} -NTT operations, the i -th Butterfly Unit's twiddle-factor is constant, given by $W_{2N_2}^i$. This twiddle factor remains unchanged across all stages of the NTT process. Consequently, the ten-step NTT method employs a fixed set of twiddle factors for every Butterfly Unit in each limb, facilitating the design of a hierarchical NTT architecture.

We can design the specific NTTU to accelerate the NTT-related computation based on the above algorithm understanding. As shown in Figure 5, the workflow of NTTU can be organized into 7 stages, which are as follows.

- N_{11} -NTT computation. During the computation of N_{11} -NTT, NTTU fetches multiple rows of one limb. Each lane processes one row by dividing it into N_{11} rows, where each row contains N_{22} elements. This ensures that the total number of elements in each row is equal to N_1 , where $N_{11} \times N_{12} = N_1$. To handle 16 elements simultaneously, *Taiyi* utilizes 16 lanes. As a result, the hardware of the N_{11} -NTT undergoes a full-pipeline process for rows of limbs. Each lane has a butterfly layer depth of 4 and 8 butterfly units per layer.

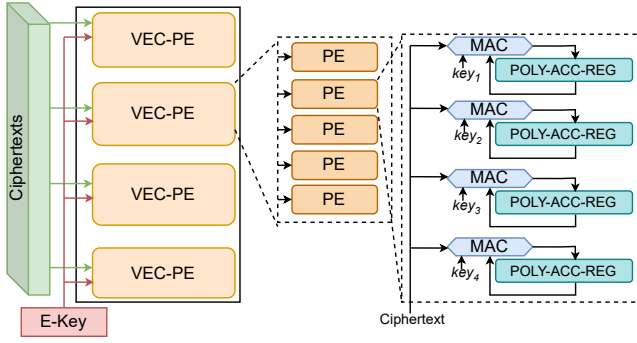


Fig. 6. Illustration of the VEC-PE array structure.

- N_1 Intra-Transpose. *Taiyi* conducts a transpose operation on the sub-rows of the limb for program execution legality. This is achieved using quadrant swap units (Quad.) and a Hadamard Product. The Quad units in each lane perform the transpose operation, featuring 18 quad units ranging from 16×16 to 2×2 . Simultaneously, the Hadamard Product manages the multiplicative operation for each element, with the necessary twist factor generated by the OF-Twist units [23]. For this stage, we implement the full-pipelined quad unit proposed in [35].
- N_{12} -NTT computation. This stage uses the same hardware configuration as N_{11} -NTT computation, but with a different twiddle factor, utilizing $W_{2N_2}^i$ as the fixed twiddle factor based on the index of the butterfly unit.
- Transpose with Buffer. In this stage, the limbs are transposed, organizing the values in row-wise. Subsequently, the above process performs Hadamard Product operations. Once all rows are stored in the buffer, the subsequent process reads them column-wise.
- N_{21} -NTT computation. Based on our previous algorithmic inference, we can deduce that this operation exhibits similar hardware behavior to both the N_{11} -NTT and N_{12} -NTT operations. The twiddle factor also remains consistent with the N_{12} -NTT operation, and the twiddle factor for each limb's computation is fixed.
- N_2 Intra-Transpose. For this stage, the hardware behavior mirrors of N_1 Intra-Transpose. The twist factor differs from the preceding operation, as it is based on W_{N_2} .
- N_{22} -NTT computation. In this stage, the hardware structure, behavior, and twiddle factor remain consistent with N_{21} -NTT computation. All twiddle factors are fixed and do not vary based on our previous algorithm inference.

Our NTTU design minimizes on-chip communication and removes the requirement for additional twiddle factors generation by algorithmic inference and profound understanding. This design choice positions our NTTU to markedly improve the performance of the NTT operation.

B. High Parallelism computation for IP operation.

As depicted in the Figure 7, the data undergoes operation *Gadget-decomp* (Figure 7(a)) before proceeding to operation *IP* (Figure 7(b)) operation, followed by operations *Recover-limbs* and *ModDown* (Figure 7(c)). It was previously noted that operation *IP* is the bottleneck of KLSS. Therefore,

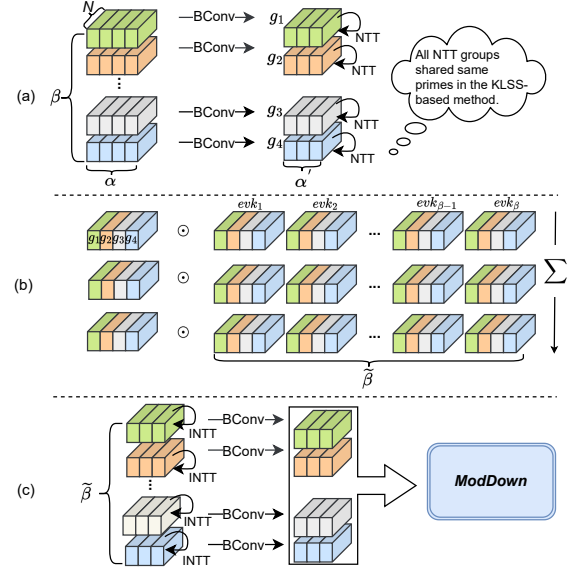


Fig. 7. The workflow and data mapping of the KLSS-based KeySwitch method. (a) The operations organization of *Gadget-decomp*. (b) *IP* operations for the KLSS-based KeySwitch, and the data organization used in *Taiyi*. (c) *Recover-Limbs* and *ModDown* operations used in the KLSS-based KeySwitch.

Taiyi introduces *HP-IP*, a dedicated component designed for parallel *IP* operations. Comprising the VEC-PE array and the *E-Key Buffer*, *HP-IP* executes element-wise multiplication using multiple MAC units, while the *E-Key Buffer* stores and prefetches keys for *IP* operations. Subsequent sections provide detailed insights into each constituent of *HP-IP*.

1) *VEC-PE array*: As illustrated in Figure 6, the VEC-PE array comprises M VEC-PEs, each of which incorporates H processing elements (PEs). In each cycle, every one of the 256 PE units located at the same horizontal position receives a data element (36-bit used in this paper). These 256 data elements pertain to the same batch of polynomials and will undergo multiplication with the corresponding elements of the key. Subsequently, it is notable that the same PE will share these data elements.

To efficiently calculate *IP* operations, we utilize data flow planning to reuse the input ciphertext during the *IP* calculation process. For each PE, consisting of 6 MAC units, following an output-stationary architecture, each MAC unit serves a distinct *E-Key*, while all sharing the same prime and input limbs. The input limbs are directed into the PE. Within each MAC unit, the same batch of polynomials undergoes multiplication with the key's elements. Subsequently, the results are aggregated in the 128-bit POLY-ACC-REG. To facilitate more efficient computations and reduce the need for frequent parameter switching during module operation, our design ensures that each MAC unit in the PE receives limbs from different groups at the same location. This approach significantly enhances the efficiency of KeySwitch.

As depicted in Figure 7(b), the dataflow of the VEC-PE involves performing vector-wise operations for PEs at the granularity of the ciphertext group. Each VEC-PE contains

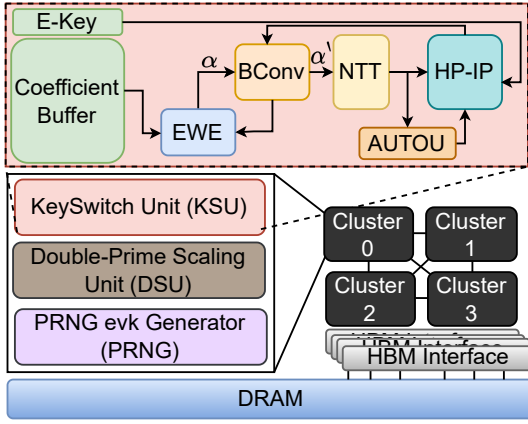


Fig. 8. The overall architecture of *Taiyi* and the dataflow for the `KeySwitch` operation. The `AUTOU`, `DSU`, and `PRNG` components are consistent with those in `SHARP` [22] `DSU` executes the `Double Scale` operation to achieve more high precision [1], [22], `PRNG` generates the key required by the `HPIP` [22], [36].

H PEs. These PEs execute limbs from different groups in parallel; PE_0 computes g_0 to g_5 , while PE_1 handles g_6 to g_{11} . It's worth noting that while increasing H enhances performance, it also demands higher bandwidth. Therefore, we set H to 4 to balance performance and bandwidth for `HP-IP`. In cases where $\tilde{\beta}$ is smaller than 4, our design allocates additional limbs from $\tilde{\beta}$ to different PEs to further enhance performance.

For IP operations in *Taiyi*'s `HP-IP` component, we integrate 256 `VEC-PE` units to process all elements in one batch. Each limb is divided into multiple fully-pipelined batches directed to the `HP-IP`. The component enables parallel computation of 24 batches, involving 4 input limbs and 6 keys, resulting in significant parallelism for IP operation in *Taiyi*.

2) *E-Key Buffer*: The *E-Key Buffer* is a storage unit that holds the evaluation key required for IP operations. It has a total size of $2\beta\tilde{\beta}\alpha'$ polynomials in typical, which is equivalent to 189MB for $N = 2^{16}$. We have carefully designed the dataflow for the `HP-IP` component to reduce memory size. By operating on 24 batches in parallel, the *E-Key Buffer* now stores only the necessary essential batches for its computation. This adjustment, aligned with the `HP-IP` component's requirements, allows *Taiyi* to allocate a 6.75MB *E-Key Buffer* for each cluster ⁴.

C. Dataflow optimization for the `KLSS KeySwitch`

Based on the dataflow illustrated in Figure 7, *Taiyi* integrates specialized components for executing the `KLSS-based KeySwitch` operation, thereby directly enhancing the performance of FHE applications. To optimize these components, we propose an efficient data-flow scheme (Figure 8). For the `KeySwitch` operation within the `HMULT` operation, the accelerator follows the computation pattern of `BConvU` \rightarrow `NTTU` \rightarrow `HP-IP` (To support Figure 7(a),(b)). Additionally, during the execution of the `BSGS` operation in bootstrapping, the accelerator selects the datapath of `AUTOU` to execute the

⁴The *E-Key Buffer* can store up to 6144 (256 \times 24 batches per computation) batches to accommodate pipeline overlap delays, enabling `HP-IP` to perform 256 continuous computations.

computation pattern of `BConvU` \rightarrow `NTTU` \rightarrow `AUTOU` \rightarrow `HP-IP`. This dataflow significantly improves the performance of `BSGS` [2]. Additionally, other hardware units schedule corresponding components based on the software stack's execution and retrieve data from the relevant storage units.

1) *Reduction of BConv operation*: As outlined in Sections III-A and III-C, the `KLSS` method exhibits an increased computational load in the `BConv` operation compared to the previous method. To address this added overhead, optimization techniques are deemed necessary.

A detailed analysis of the `KLSS` method's workflow reveals that the *Recover-Limbs* stage significantly contributes to the augmented `BConv` operation. In this stage, a total of $\tilde{\beta}$ `BConv` operations are conducted to convert limbs from R^T to R^{PQ} . For the last group, two consecutive `BConv` operations are performed on the limbs: the first to transition from R^T to R^P and the second for the transform to R^Q for the `ModDown` operation. Consequently, we propose a direct conversion of the last group's limbs from R^T to R^Q to optimize the execution of the `ModDown` operation.

$$\begin{aligned} a_{R^P} &\approx \text{BConv}_{T \rightarrow P}(a_{R^T}) = a_{R^P} + Te_1 \\ a_{R^Q} &\approx \text{BConv}_{P \rightarrow Q}(a_{R^P}) = a_{R^Q} + Te_1 + Pe_2 \quad (9) \\ \implies a_{R^Q} &\approx \text{BConv}_{T \rightarrow P}(a_{R^T}) = a_{R^Q} + Te \end{aligned}$$

Noise reduction: The `BConv` operation is an approximate scheme based on the Chinese Remainder Theorem (CRT), which introduces noise bias once for each transforms [10]. As depicted in Eq. 9, the conversion from R^T to R^P leads to the introduction of T-fold noise. Consequently, two consecutive conversions result in the accumulation of two types of noise, R^T and R^P . Hence, as shown in Eq. 9, we propose to streamline the operation for the *Recover-Limbs* stage, aiming to mitigate the noise caused by the `BConv` operation.

2) *PtMatVecMult optimization*: The `PtMatVecMult` operation, pivotal in `Bootstrapping`, undergoes optimization via the `KLSS` method, employed in *CoeffToSolt* and *SoltToCoeff* operations. The operation applies `BConv` to transform limbs into R^T , followed by r sets of operation groups, each comprising two `Automorph` and one IP operation. Limbs then undergo `ModDown` to reduce the multiplicative level.

Through these optimizations and the designed workflow for *Taiyi*, we achieve high performance in `KLSS-based FHE` applications. Strategies focus on streamlining batch-level data flow and minimizing redundant `NTT` operations, resulting in exceptional performance in executing applications on *Taiyi*.

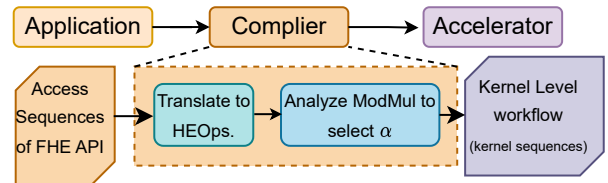


Fig. 9. The overall workflow of the Compiler-assisted optimization for the FHE applications.

TABLE V
CKKS INSTANCE PARAMETER USED FOR EVALUATION.

Parameter	N	L	d_{num}	α	α'	β	L_{eff}
Value	2^{16}	38	6	Dynamic	4	$\frac{L+\alpha}{\alpha}$	17

D. Compiler-assisted optimization for α for FHE applications

We develop a compiler for CKKS FHE applications to optimize performance for varying multiplicative levels. As shown in Figure 9, this compiler operates in two steps: 1) It translates requests from applications into FHE operations. 2) It analyzes the number of ModMul times, selects α values for each level based on N, and generates kernel sequences associated with distinct α values for different levels, as explained in Section III-D. Therefore, when a ciphertext undergoes a `keyswitch` operation, the alpha value is selected based on the limb count without additional switching time.

V. METHODOLOGY

We implement all components of *Taiyi* in Verilog using the TSMC 7nm Processing Design Kit (PDK) [28]. These components are designed with full pipelining and operate at a frequency of 1GHz. Additionally, we have incorporated the SRAM components provided by the PDK.

We constructed a cycle-level simulator based on the SimFHE [2] for *Taiyi*, consisting of two core components: the *Instruction Generator* and the *Hardware Executor*. The former executes FHE applications, generating a sequence of HE operations. These operations are then transformed into a data dependence graph of *Arithmetic* kernels, subsequently sent to the *Hardware Executor* for hardware behavior simulation. The *Hardware Executor* selects appropriate components based on the calculation graph and tracks the frequency of their execution by processing the data flow received from the *Instruction Generator*. Concurrently, it calculates the time needed to execute instructions based on the pipeline depth of the components and the total number of instructions.

We conducted runtime measurements for bootstrapping and representative FHE CKKS workloads by the simulator. To optimize performance and maintain a 128-bit security level, we applied KLSS methods [24]. As demonstrated in Table V, through the collaborative analysis of the new algorithm and hardware in Section III-B, we have identified parameters that can efficiently execute FHE applications. The utilized open-sourced workloads are:

- **Bootstrapping [31]:** This example involves performing bootstrapping operations, which consumes the multiplicative $L_{\text{boot}} = 21$ [31].
- **HELR1024 [2], [17]:** For this application, we trained a logistic regression (LR) model on binary classification data using the FHE CKKS scheme [17].
- **ResNet-20 [26]:** We employed the FHE CKKS implementation of the ResNet-20 [27] model from [26], applying it to $32 \times 32 \times 3$ CIFAR-10 [26] images for once CNN inference.

The selected applications encompass a variety of tasks, effectively demonstrating the versatility and functionality of

TABLE VI
RESOURCE PARAMETER IN FHE ACCELERATORS: BANDWIDTH (BW) AND CAPACITY (CAP) METRICS. ALL ACCELERATOR WORKING AT 1GHZ OPERATION FREQUENCY.

	Crater+	BTS	ARK	Sharp	<i>Taiyi</i>
# of lanes	2048	2048	1024	1024	1024
On-chip Mem Cap (MB)	256	512	512	180	128.25
On-chip Mem BW (TB/S)	84	-	92	72	75
Power (W)	-	163.2	281	98	80
Area (mm ²)	222.7	373.6	418.3	178.8	151.6

our proposed ASIC accelerator. To provide a more detailed illustration of *Taiyi*'s performance, we simulate both serial and parallel modes as follows.

- **Sharp_{Serial}:** Implements the optimization methods described in this paper on Sharp [22], with each component executing sequentially and without overlap.
- ***Taiyi*_{Serial}:** Implements the optimization methods outlined in this paper on *Taiyi*, with each component executing sequentially and without any overlap.
- ***Taiyi*_{Parallel}:** Implement the optimization method outlined in this article on *Taiyi*, where computing components can be executed concurrently.

In the serial mode, the accelerator's components execute sequentially, with only one component running in each cycle. In contrast, the parallel mode allows all components to execute simultaneously on the accelerator. For example, HPIP can process the output of NTTU concurrently with NTTU processing other input data.

VI. RESULTS

A. Performance and Efficiency Analysis of *Taiyi*

This section comprehensively explains the optimization approach to enhance FHE application performances. The performance evaluation of *Taiyi* is conducted, including execution time and chip area, compared to previous designs. Table VI illustrates that *Taiyi* outperforms Crater+, BTS, ARK, and Sharp, exhibiting reductions of 31.9%, 59.4%, and 63.7%, and 15.7% in chip area, respectively. Furthermore, *Taiyi* attains bandwidth reductions of 1.12 \times and 1.22 \times in comparison to Crater+ and ARK, respectively. Compared to Sharp, *Taiyi* experiences only a 4.16% increase in bandwidth requirements. Besides, we also reduce 28.75% on-chip memory requirement compared to the previous minimum accelerator.

As shown in Table VII, *Taiyi* achieves an average performance improvement of 1.17 \times in serial mode compared to Sharp_{Serial}. This result indicates that the optimized hardware design efficiently executes FHE applications without algorithm optimization, demonstrating that the optimized NTTU and designed HP-IP components enhance FHE application execution efficiency. Additionally, *Taiyi*_{Parallel} achieves 2.83 \times and 1.54 \times performance improvement compared to *Taiyi*_{Serial} and the previous state-of-the-art (SOTA) [22]. This achievement suggests that *Taiyi* exhibits strong concurrency, capable of executing multiple components simultaneously. Hardware and algorithm optimizations reduce the execution time of the

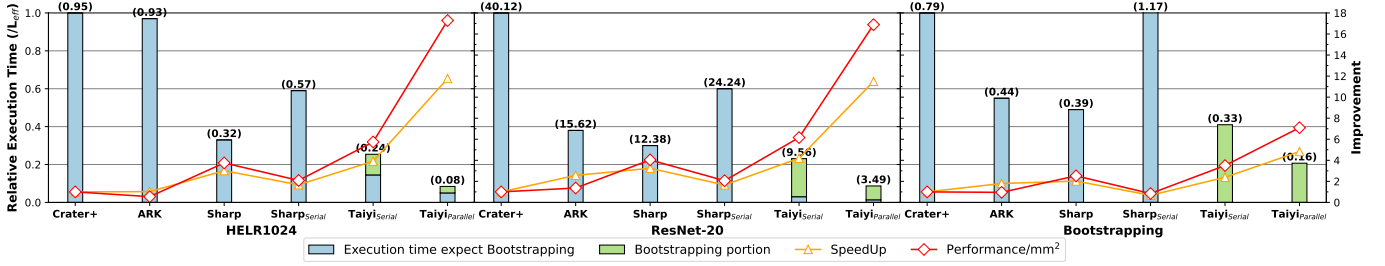


Fig. 10. Performance Comparison of *Taiyi* with Prior Accelerators. Evaluation within HELR1024, ResNet-20, and Bootstrapping (Normalized by L_{eff})

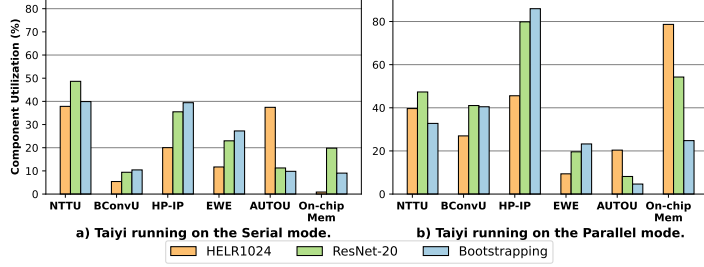


Fig. 11. Utilization of *SolutionName* Components.

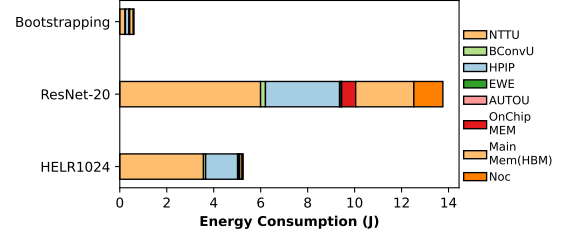


Fig. 12. Energy Consumption of *SolutionName* Components.

TABLE VII

COMPARISON OF ABSOLUTE PERFORMANCE BETWEEN *Taiyi* AND OTHER PRIOR WORKS (MS).

	HELR1024	ResNet-20	Bootstrapping	L_{eff}
CPU	23.3(s)	2271(s)	17.2(s)	8
Crater+	7.62	321	6.32	8
ARK	7.42	125	3.52	8
Sharp	2.53	99	3.12	8
Sharp _{Serial}	4.54	193.89	9.35	8
Taiyi _{Serial}	4.14	162.60	7.61	17
Taiyi _{Parallel}	1.37	59.33	2.77	17

KeySwitch operation by optimizing α and decreasing the execution times of NTT and BConv operations.

As indicated in Table VII, our design exhibits higher L_{eff} after security analysis, demonstrating its ability to perform more effective multiplications for various FHE applications. Therefore, as illustrated in Figure 10, we further evaluate the efficiency of application execution time. A lower allocation time signifies more effective execution of FHE operations, suggesting that our design can achieve better execution efficiency for a wider range of FHE applications. *Taiyi* achieves a performance improvement of $7.04\times$ compared to Sharp_{Serial}. Besides, it achieves a 68.1% performance improvement compared to the results reported in Sharp [22].

We conducted a comparison of performance per area with previous designs. The results show that our design can achieve an average improvement of $13.75\times$, $17.13\times$, $3.87\times$, and $8.31\times$ for Crater+, ARK, Sharp, and Sharp_{Serial}.

Figure 10 illustrates that the Bootstrapping operation constitutes the primary overhead in FHE applications, accounting for 84.3% and 40.7% for ResNet-20 and HELR1024, respectively. Hence, it remains the principal source of overhead in the KLSS-based method.

B. Component Utilization and Energy Consumption Analysis

This section focuses on the computation components (NTTU, BConvU, HP-IP, EWE, and AutoU) for analyzing

utilization and energy consumption per area. As depicted in Figure 11, for the serial mode, HP-IP emerges as the most utilized component in Bootstrapping applications, achieving 39.4% . The utilization of NTTU, HP-IP, and EWE in all applications is substantial, averaging 31.47% . This observation indicates that our design and optimization efforts achieve a balanced utilization across all components in executing FHE applications. In the parallel mode, the HP-IP achieves 85.94% utilization for the Bootstrapping operation and an average utilization of 70.45% across the above FHE applications. This indicates that the HP-IP can be efficiently utilized during the execution of FHE applications. Additionally, the other components also achieve a balanced utilization during application execution.

Furthermore, we provide energy consumption data for applications on *Taiyi*, demonstrating that *Taiyi* consumes low power. As shown in Figure 11, ResNet-20 only consumes 5.99J on NTT, with HP-IP consuming 3.15J . These results affirm that *Taiyi* is a low-power accelerator, dissipating less than 80W of power for all FHE applications.

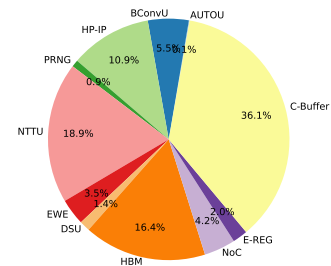


Fig. 13. Breakdown of accelerator area, indicating the distribution of resources among key components: C-Buffer (36.1%), HP-IP (10.9%), NTTU (18.9%), BConv (5.5%), and Others (28.6%).

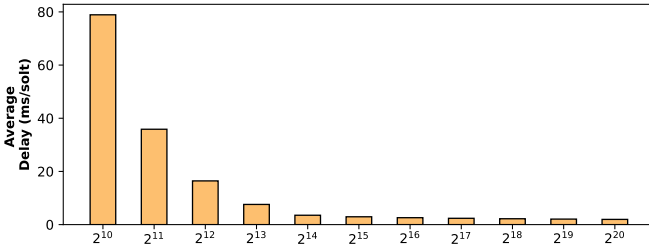


Fig. 14. Execution Time per solt for different N within *Taiyi*.

C. Accelerator area breakdown

As depicted in Figure 13, the predominant area within the accelerator is occupied by storage-related components, comprising up to 38.15%. This observation underscores the substantial storage demands inherent in the FHE accelerator hardware design. If only increasing EWE of sharp [22] will significantly increase the chip area. Therefore, the HP-IP component represents a modest 10.9% of the total area, resulting in a significant 74.2% reduction in area overhead compared to equivalent EWE units with similar parallelism. This efficiency is achieved through the shared utilization of compute units for the same limbs within the HP-IP.

D. Sensitivity Study

1) *Impact of N on Optimal NTT Operation:* In this section, to comprehensively assess the performance of NTTU in *Taiyi*, we conducted evaluations across polynomials of varying degrees. We analyzed the average computation delay for each modulus multiplication. As depicted in Figure 14, the average computation time decreases with increased polynomial length. However, when the length reaches 2^{16} , the rate of descent begins to slow down, suggesting that our design effectively supports calculations with polynomial lengths of 2^{16} and maintains robust computational performance for longer polynomials.

2) *Impact of α on Optimal BConv Operation:* In this section, we conducted evaluations with varying α values to analyze the computational performance of the optimized algorithm. As illustrated in Figure 15, it is evident that as α increases, the reduction in computational workload also increases. Consequently, we can infer that the optimization algorithm proposed in this work is versatile, supporting any length of α and effectively reducing computational complexity.

VII. RELATED WORK

A. GPU and FPGA acceleration method for FHE

Numerous research efforts [3], [14], [21], [37], [39], [40] have aimed to accelerate FHE applications on GPU and FPGA platforms. In the pioneering work by Ref. [21], FHE CKKS received initial GPU support, demonstrating a significant reduction in off-chip memory access through kernel fusion across primary functions. The work by Ref. [14] introduced the use of tensor cores in recent NVIDIA GPUs for NTT acceleration, employing an approach that breaks down each 32-bit word into 8-bit integers fed into tensor cores. Despite this innovative technique, GPUs' limited on-chip memory

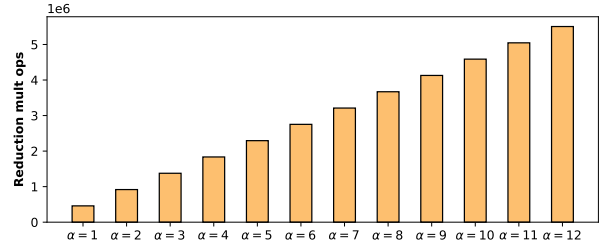


Fig. 15. Multiplication operation number reduction with different α .

capacity still results in frequent off-chip memory accesses, leading to memory-bound FHE workloads. Addressing this challenge, Ref. [3] optimized the dataflow of the *KeySwitch* operation on FPGA, effectively overcoming the memory bandwidth bottleneck. Additionally, Ref. [40] achieved notable performance enhancements for FHE applications through algorithm optimizations and modular fusion. Further contributions from research efforts like Ref. [15], [32], [41] have accelerated application performance, particularly focusing on the TFHE scheme and deploying dedicated circuit designs for NTT/FFT operations. Despite the significant strides in these endeavors to accelerate FHE, a substantial performance gap persists, hindering the development of FHE.

B. ASIC accelerator design for FHE

Several domain-specific accelerators have been proposed to enhance the practical performance of FHE applications, as detailed in works such as [2], [22], [23], [25], [35], [36]. The first ASIC implementation supporting the CKKS scheme is presented in Ref. [35]. However, it exhibits a performance gap in executing FHE applications and lacks support for the bootstrapping operation. Contrarily, [25], [36] optimize FHE applications through parameter selection, achieving comparable performance for bootstrapping and becoming the first to execute applications with unbounded multiplicative depth. [23] focuses on optimizing the BSGS operation using bootstrapping, significantly reducing the memory requirement of the bootstrapping operation. The state-of-the-art accelerator implementation for the CKKS scheme is Ref. [22], which reduces on-chip memory size by decreasing the word length from the precision of real-world applications. It achieves optimal performance by enhancing the parallelism of the BConv component. Another optimization effort is presented by Ref. [2], which optimizes the dataflow to reduce on-chip memory requirements and also mitigates NTT operations. Additionally, Ref. [20], [33], [38] contribute to accelerating TFHE applications by improving the performance of the blind-rotate operation through parallelization. Despite these notable acceleration efforts, these works still encounter performance bottlenecks for the KLSS method.

VIII. CONCLUSION

This paper introduces the *Taiyi*, an accelerator specifically designed for KLSS-based FHE applications. We comprehensively analyze the computational workload differences between the KLSS-based *KeySwitch* method and the previous method. Our accelerator features dedicated hardware for

the Inner-product operation, which ensures high performance while minimizing on-chip bandwidth requirements. Algorithmic optimizations are proposed to reduce the computational burden of the BConv operation. Additionally, we present a static compiler designed to dynamically select the optimal α during the runtime of FHE applications.

Taiyi demonstrates high efficiency compared to state-of-the-art ASIC FHE accelerators designed for KLSS-based methods, showcasing a $3.8\times$ enhancement in performance per area. This emphasizes the effectiveness of our design in addressing the specific computational challenges associated with KLSS-based FHE applications.

REFERENCES

- [1] R. Agrawal, J. H. Ahn, F. Bergamaschi, R. Cammarota, J. H. Cheon, F. DM de Souza, H. Gong, M. Kang, D. Kim, J. Kim *et al.*, “High-precision rms-ckks on fixed but smaller word-size architectures: theory and application,” in *Proceedings of the 11th Workshop on Encrypted Computing & Applied Homomorphic Cryptography*, 2023, pp. 23–34.
- [2] R. Agrawal, L. de Castro, G. Juvekar, A. Chandrakasan, V. Vaikuntanathan, and A. Joshi, “Mad: Memory-aware design techniques for accelerating fully homomorphic encryption,” in *The 56th IEEE/ACM International Symposium on Microarchitecture (MICRO)*. IEEE, 2023.
- [3] R. Agrawal, L. de Castro, G. Yang, C. Juvekar, R. Yazicigil, A. Chandrakasan, V. Vaikuntanathan, and A. Joshi, “Fab: An fpga-based accelerator for bootstrappable fully homomorphic encryption,” in *2023 IEEE International Symposium on High-Performance Computer Architecture (HPCA)*. IEEE, 2023, pp. 882–895.
- [4] J.-C. Bajard, J. Eynard, M. A. Hasan, and V. Zucca, “A full rms variant of fv like somewhat homomorphic encryption schemes,” in *Selected Areas in Cryptography–SAC 2016: 23rd International Conference, St. John’s, NL, Canada, August 10–12, 2016, Revised Selected Papers*. Springer, 2017, pp. 423–442.
- [5] F. Boemer, A. Costache, R. Cammarota, and C. Wierzynski, “ngraph-2: A high-throughput framework for neural network inference on encrypted data,” in *Proceedings of the 7th ACM Workshop on Encrypted Computing & Applied Homomorphic Cryptography*, 2019, pp. 45–56.
- [6] Z. Brakerski, C. Gentry, and V. Vaikuntanathan, “(leveled) fully homomorphic encryption without bootstrapping,” *ACM Transactions on Computation Theory (TOCT)*, vol. 6, no. 3, pp. 1–36, 2014.
- [7] Z. Brakerski and V. Vaikuntanathan, “Efficient fully homomorphic encryption from (standard) lwe,” *SIAM Journal on computing*, vol. 43, no. 2, pp. 831–871, 2014.
- [8] H. Chen, I. Chillotti, and Y. Song, “Improved bootstrapping for approximate homomorphic encryption,” in *Annual International Conference on the Theory and Applications of Cryptographic Techniques*. Springer, 2019, pp. 34–54.
- [9] H. Chen, W. Dai, M. Kim, and Y. Song, “Efficient multi-key homomorphic encryption with packed ciphertexts with application to oblivious neural network inference,” in *Proceedings of the 2019 ACM SIGSAC Conference on Computer and Communications Security*, 2019, pp. 395–412.
- [10] J. H. Cheon, K. Han, A. Kim, M. Kim, and Y. Song, “A full rms variant of approximate homomorphic encryption,” in *Selected Areas in Cryptography–SAC 2018: 25th International Conference, Calgary, AB, Canada, August 15–17, 2018, Revised Selected Papers 25*. Springer, 2019, pp. 347–368.
- [11] I. Chillotti, N. Gama, M. Georgieva, and M. Izabachène, “Tfhe: fast fully homomorphic encryption over the torus,” *Journal of Cryptology*, vol. 33, no. 1, pp. 34–91, 2020.
- [12] L. de Castro, R. Agrawal, R. Yazicigil, A. Chandrakasan, V. Vaikuntanathan, C. Juvekar, and A. Joshi, “Does fully homomorphic encryption need compute acceleration?” *arXiv preprint arXiv:2112.06396*, 2021.
- [13] J. Fan and F. Vercauteren, “Somewhat practical fully homomorphic encryption,” *Cryptology ePrint Archive*, 2012.
- [14] S. Fan, Z. Wang, W. Xu, R. Hou, D. Meng, and M. Zhang, “Tensorfhe: Achieving practical computation on encrypted data using gpgpu,” in *2023 IEEE International Symposium on High-Performance Computer Architecture (HPCA)*. IEEE, 2023, pp. 922–934.
- [15] S. Gener, P. Newton, D. Tan, S. Richelson, G. Lemieux, and P. Brisk, “An fpga-based programmable vector engine for fast fully homomorphic encryption over the torus,” in *SPSL: Secure and Private Systems for Machine Learning (ISCA Workshop)*, 2021.
- [16] Y. Ha, “Sparselwe-estimator,” <https://github.com/Yongyongha/SparseLWE-estimator>, 2021.
- [17] K. Han, S. Hong, J. H. Cheon, and D. Park, “Logistic regression on homomorphic encrypted data at scale,” in *AAAI Conference on Artificial Intelligence (AAAI)*, 2019, pp. 9466–9471.
- [18] K. Han and D. Ki, “Better bootstrapping for approximate homomorphic encryption,” in *Topics in Cryptology–CT-RSA 2020: The Cryptographers’ Track at the RSA Conference 2020, San Francisco, CA, USA, February 24–28, 2020, Proceedings*. Springer, 2020, pp. 364–390.
- [19] I. Hwang, J. Seo, and Y. Song, “Optimizing he operations via level-aware key-switching framework,” *Cryptology ePrint Archive*, 2023.
- [20] L. Jiang, Q. Lou, and N. Joshi, “Matcha: A fast and energy-efficient accelerator for fully homomorphic encryption over the torus,” in *Proceedings of the 59th ACM/IEEE Design Automation Conference*, 2022, pp. 235–240.
- [21] W. Jung, S. Kim, J. H. Ahn, J. H. Cheon, and Y. Lee, “Over 100x faster bootstrapping in fully homomorphic encryption through memory-centric optimization with gpu,” *IACR Transactions on Cryptographic Hardware and Embedded Systems*, pp. 114–148, 2021.
- [22] J. Kim, S. Kim, J. Choi, J. Park, D. Kim, and J. H. Ahn, “Sharp: A short-word hierarchical accelerator for robust and practical fully homomorphic encryption,” in *Proceedings of the 50th Annual International Symposium on Computer Architecture*, 2023, pp. 1–15.
- [23] J. Kim, G. Lee, S. Kim, G. Sohn, J. Kim, M. Rhu, and J. H. Ahn, “Ark: Fully homomorphic encryption accelerator with runtime data generation and inter-operation key reuse,” *arXiv preprint arXiv:2205.00922*, 2022.
- [24] M. Kim, D. Lee, J. Seo, and Y. Song, “Accelerating HE operations from key decomposition technique.” *CRYPTO 2023*.
- [25] S. Kim, J. Kim, M. J. Kim, W. Jung, J. Kim, M. Rhu, and J. H. Ahn, “Bts: An accelerator for bootstrappable fully homomorphic encryption,” in *Proceedings of the 49th Annual International Symposium on Computer Architecture*, 2022, pp. 711–725.
- [26] E. Lee, J.-W. Lee, J. Lee, Y.-S. Kim, Y. Kim, J.-S. No, and W. Choi, “Low-complexity deep convolutional neural networks on fully homomorphic encryption using multiplexed parallel convolutions,” in *International Conference on Machine Learning (ICML)*, 2022, pp. 12403–12422.
- [27] J.-W. Lee, H. Kang, Y. Lee, W. Choi, J. Eom, M. Deryabin, E. Lee, J. Lee, D. Yoo, Y.-S. Kim *et al.*, “Privacy-preserving machine learning with fully homomorphic encryption for deep neural network,” *IEEE Access*, vol. 10, pp. 30039–30054, 2022.
- [28] M. Liu, “1.1 unleashing the future of innovation,” in *2021 IEEE International Solid-State Circuits Conference (ISSCC)*, vol. 64. IEEE, 2021, pp. 9–16.
- [29] Q. Lou, B. Feng, G. Charles Fox, and L. Jiang, “Glyph: Fast and accurately training deep neural networks on encrypted data,” *Advances in neural information processing systems*, vol. 33, pp. 9193–9202, 2020.
- [30] Q. Lou and L. Jiang, “Hemet: A homomorphic-encryption-friendly privacy-preserving mobile neural network architecture,” in *International conference on machine learning*. PMLR, 2021, pp. 7102–7110.
- [31] C. Mouchet, J.-P. Bossuat, J. Troncoso-Pastoriza, and J. Hubaux, “Lattigo: A multiparty homomorphic encryption library in go,” in *WAHC 2020–8th Workshop on Encrypted Computing & Applied Homomorphic Cryptography*, 2020.
- [32] K. Nam, H. Oh, H. Moon, and Y. Paek, “Accelerating n-bit operations over tthe on commodity cpu-fpga,” in *Proceedings of the 41st IEEE/ACM International Conference on Computer-Aided Design*, ser. ICCAD ’22. New York, NY, USA: Association for Computing Machinery, 2022. [Online]. Available: <https://doi.org/10.1145/3508352.3549413>
- [33] A. Putra, Y. Chen, J. Kim, J.-Y. Kim *et al.*, “Strix: An end-to-end streaming architecture with two-level ciphertext batching for fully homomorphic encryption with programmable bootstrapping,” *arXiv e-prints*, pp. arXiv–2305, 2023.
- [34] M. S. Riazi, K. Laine, B. Pelton, and W. Dai, “Heax: An architecture for computing on encrypted data,” in *Proceedings of the Twenty-Fifth International Conference on Architectural Support for Programming Languages and Operating Systems*, 2020, pp. 1295–1309.
- [35] N. Samardzic, A. Feldmann, A. Krastev, S. Devadas, R. Dreslinski, C. Peikert, and D. Sanchez, “F1: A fast and programmable accelerator

- ator for fully homomorphic encryption,” in *MICRO-54: 54th Annual IEEE/ACM International Symposium on Microarchitecture*, 2021, pp. 238–252.
- [36] N. Samardzic, A. Feldmann, A. Krastev, N. Manohar, N. Genise, S. Devadas, K. Eldefrawy, C. Peikert, and D. Sanchez, “Craterlake: a hardware accelerator for efficient unbounded computation on encrypted data,” in *ISCA*, 2022, pp. 173–187.
- [37] K. Shividikar, Y. Bao, R. Agrawal, M. Shen, G. Jonatan, E. Mora, A. Ingare, N. Livesay, J. L. Abellán, J. Kim *et al.*, “Gme: Gpu-based microarchitectural extensions to accelerate homomorphic encryption,” *arXiv preprint arXiv:2309.11001*, 2023.
- [38] M. Van Beirendonck, J.-P. D’Anvers, and I. Verbauwhede, “Fpt: a fixed-point accelerator for torus fully homomorphic encryption,” *arXiv preprint arXiv:2211.13696*, 2022.
- [39] Z. Wang, P. Li, R. Hou, Z. Li, J. Cao, X. Wang, and D. Meng, “He-booster: An efficient polynomial arithmetic acceleration on gpus for fully homomorphic encryption,” *IEEE Transactions on Parallel and Distributed Systems*, vol. 34, no. 4, pp. 1067–1081, 2023.
- [40] Y. Yang, H. Zhang, S. Fan, H. Lu, M. Zhang, and X. Li, “Poseidon: Practical homomorphic encryption accelerator,” in *2023 IEEE International Symposium on High-Performance Computer Architecture (HPCA)*. IEEE, 2023, pp. 870–881.
- [41] T. Ye, R. Kannan, and V. K. Prasanna, “Fpga acceleration of fully homomorphic encryption over the torus,” in *2022 IEEE High Performance Extreme Computing Conference (HPEC)*. IEEE, 2022, pp. 1–7.